Detecting climate variability impacts on reference and actual evapotranspiration in the Taohe River Basin, NW China

Linshan Yang, Qi Feng, Changbin Li, Jianhua Si, Xiaohu Wen and Zhenliang Yin

ABSTRACT

Analysis of the impacts of climate variability on evapotranspiration (*ET*) is of great importance in understanding climate variability and its effect on hydrological aspects. In this study, temporal and spatial variations in reference evapotranspiration (ET_0) and actual evapotranspiration (*AET*) were comprehensively detected in the Taohe River Basin from 1981 to 2010. The spatial distributions of annual sensitivity of ET_0 and *AET* to climatic variables were investigated. The quantitative contributions, the possible causes and dominant controlling factors were analyzed. The results suggested the following. (1) Considerable changes in ET_0 occurred due to climate variability in the Gannan Plateau area (GPA) and Loess Plateau area (LPA) by 3.54 mm/yr and 3.39 mm/yr from 1981 to 2010, respectively. (2) Net solar radiation was the most sensitive factor on ET_0. The dominant factor was air temperature leading to increase in ET_0 due to high sensitive coefficient to ET_0 and also exhibited significant increasing magnitude. (3) Precipitation (*PPT*) was the most sensitive factor for *AET*. *AET* in the GPA is controlled by air temperature and in LPA is controlled by *PPT*. This study provides a beneficial reference to agriculture, water resource and eco-environment management strategies in this region for associated policymakers and stakeholders.

Key words | actual evapotranspiration, climate variability impacts, reference evapotranspiration, sensitivity coefficient, Taohe River Basin

Linshan Yang
Qi Feng (corresponding author)
Jianhua Si
Xiaohu Wen
Zhenliang Yin
Cold and Arid Regions Environmental and Engineering Research Institute, Chinese Academy of Sciences,
Lanzhou 730000,
China
and
Key Laboratory of Ecohydrology of Inland River Basin,
Chinese Academy of Sciences,
Lanzhou 730000,
China
E-mail: *qifeng@lzb.ac.cn*

Linshan Yang
University of Chinese Academy of Sciences,
Beijing 100049,
China

Linshan Yang
Changbin Li
College of Earth and Environmental Sciences,
Lanzhou University,
Lanzhou 730000,
China

INTRODUCTION

Evapotranspiration (*ET*) is an essential component of the hydrological cycle (Kite 2000; Mackay *et al.* 2012) and strongly influenced by climatic factors, soil characteristics, vegetation, and many other underlying surface factors, such that the controls on *ET* are very complex (Katul *et al.* 2012; Yang *et al.* 2012). *ET* accounts for some 60% of terrestrial precipitation and can approach 100% of annual rainfall in water-limited ecosystems, with transpiration often a dominant term in numerous vegetated landscapes (Teuling *et al.* 2009; Huo *et al.* 2013). In China, climate variability is the major force and increasing air temperature leads to higher evaporation rates and enables the atmosphere to transport higher amounts of water vapor, which will accelerate the hydrological cycle and cause uneven distribution of water resources (Piao *et al.* 2010; Jung *et al.* 2010). Understanding the changes in *ET* due to climate variability impact is crucial to understand the influence of climate variability on the eco-hydrological processes of complex landscapes (Matin & Bourque 2013), and may help to eliminate threats and enhance water resource management (Liu

doi: 10.2166/nh.2016.252

et al. 2010) in order to assess and manage the water budget for agricultural purposes (Liu and Luo 2010).

The Penman–Monteith (P-M) method, recommended by the Food and Agriculture Organization (FAO), combines the radiometric and aerodynamic parameters and reflects the combined effect of climate factors and terrestrial processes (Liu and Luo 2010), as a standard for estimating potential evaporation (ET_0), and is widely acknowledged as the most accurate method for both arid and humid climate areas (Allen *et al.* 1998). In recent years, considerable research efforts have been made in the field of the potential influence of climate variability on ET_0 (Liu *et al.* 2010; Cheng *et al.* 2013; Matin & Bourque 2013; Peng *et al.* 2013). Brutsaert (2013) found a decreasing pan evaporation trend of 4.57 mm per year and an increasing terrestrial evaporation trend of 0.7 mm per year from 1966 to 2000 in the Tibetan Plateau. Huo *et al.* (2013) confirmed the significant declining trend of ET_0 with a mean value of approximately 3 mm per year over the last 50 years in the arid regions of China. However, ET_0 has increased in the semi-arid regions (Tabari 2010; Tabari & Marofi 2010). The results of these analyses can allow determination of the accuracy required when using climatic variables to estimate ET_0. As it is affected by water and energy conditions and to understand the impact of key meteorological variables on evapotranspiration, it is necessary to conduct sensitivity analyses. The sensitivity of ET_0 to different climatic factors varies in different regions. Huo *et al.* (2013) reported that wind speed was the most sensitive meteorological factor for ET_0 in arid regions of China, and Gong *et al.* (2006) found relative humidity had the greatest influence on ET_0 in the humid Yangtze River Basin of China. Liu *et al.* (2010) suggested that in the Yellow River Basin, ET_0 is most sensitive to solar radiation followed by relative humidity, air temperature, and wind speed. Goyal (2004) reported that ET_0 is sensitive to air temperature and net solar radiation in arid regions of India. Xu *et al.* (2006) introduced a method by removing trends of each meteorological variable series and quantified the impact of ET_0. These studies could improve the understanding of the influence of climate variability on ET_0. However, characterizing and quantifying the influence of climate variability on *AET*, and examining the dominant controlling factors remain an ongoing and important problem. Budyko (1961, 1974) proposed a semi-empirical expression for estimating the regional long-term average annual actual evapotranspiration (*AET*) from ET_0 by analyzing a time-series of climatic data at catchment scale based on the complementary relationship coupled water-energy balance (Budyko 1974; Wang *et al.* 2013). This was defined as the Budyko hypothesis. In order to emphasize the influence of soil and landscape properties on *AET*, Fu (1981) added an analytical expression to the Budyko hypothesis. The complementary relationship between actual and potential evapotranspiration correlated via precipitation, which is derived phenomenologically mathematically provides a complete picture of the evaporation mechanism (Zhang *et al.* 2012). Using Fu's equation, the *AET* could be estimated (Yang *et al.* 2006; Jiang *et al.* 2015). Based on the Budyko hypothesis, the sensitivity and dominant controlling factors of *AET* can be discussed.

China's Taohe River Basin (TRB), a transition basin between the Qinghai-Tibet Plateau and the Loess Plateau, stretches across the eastern Tibetan Plateau (Zhang *et al.* 2002) and southwestern Loess Plateau (Yang *et al.* 1988). Due to the heterogeneity of the climate and underlying surface conditions, the eco-hydrological processes of the TRB show significant spatial-temporal heterogeneity and it is one of the most sensitive regions to climate variability in China. From the upstream reaches in the west to the downstream reaches in the northeast, the dominant climate variability from an alpine cold humid and sub-humid climate to a temperate semi-arid climate, and the terrestrial vegetation shows significant heterogeneity, ranging from alpine grasslands and forests in the upstream regions to arid woodlands and grasslands in the downstream regions (Li *et al.* 2014).

The objectives of this study are: (1) to calculate reference evapotranspiration using the P-M method and actual evapotranspiration with the Fu's equation of Budyko hypothesis; (2) to analyze the spatial distribution of the annual ET_0 and *AET* trends and their sensitivities to climatic variables; and (3) to quantify the influence of climate variability on ET_0 and *AET*, and to investigate the dominant controlling factors driving the changes in different climatic regions of TRB, China.

STUDY AREA AND DATA DESCRIPTION

The Taohe River originates from the north of Xiqing Mountain and covers a total drainage area of 25,527 km^2 between

101°36′E and 104°20′E, and 34°06′N and 36°01′N (Figure 1), with a total runoff of 46.9×10^8 m^3 per year. The river flows through the eastern Tibetan Plateau and southwestern Loess Plateau and finally reaches the LJX Reservoir, which is located in the main stream of the upper Yellow River. In the eastern Tibetan Plateau area (Gannan Plateau area, GPA), the land cover and topography change from forests and mountains to grasslands and open valleys. In the southwestern Loess Plateau area (Longxi Loess Plateau area, LPA), the vegetation cover is low (average of 22% vegetative cover), which causes severe soil erosion due to summer rainstorms and the crude soil characteristics of this region (Yang *et al.* 2014). The mean annual air temperature increases from 1 °C in the Gannan Plateau at elevations ranging from 4,562 to 2,800 m a.s.l, to 9 °C in the southwestern Loess Plateau, at elevations ranging from 2,800 to 1,731 m a.s.l. The mean annual precipitation decreases from 600 mm to 300 mm from west to east. From upstream regions in the west to downstream regions in the east, the dominant climate varies from an alpine cold humid and sub-humid climate to a temperate semi-arid climate, while the terrestrial vegetation ranges from alpine grasslands in the upstream regions to forest and arid grasslands in the downstream regions (Li *et al.* 2015).

Daily meteorological data collected in and around the TRB were provided by the National Climatic Centre of the China Meteorological Administration from January 1981 to December 2010. The data sets included daily minimum, maximum and mean air temperature, relative humidity, wind speed at 2 m, sunshine hours, and precipitation. The station information is presented in Table 1.

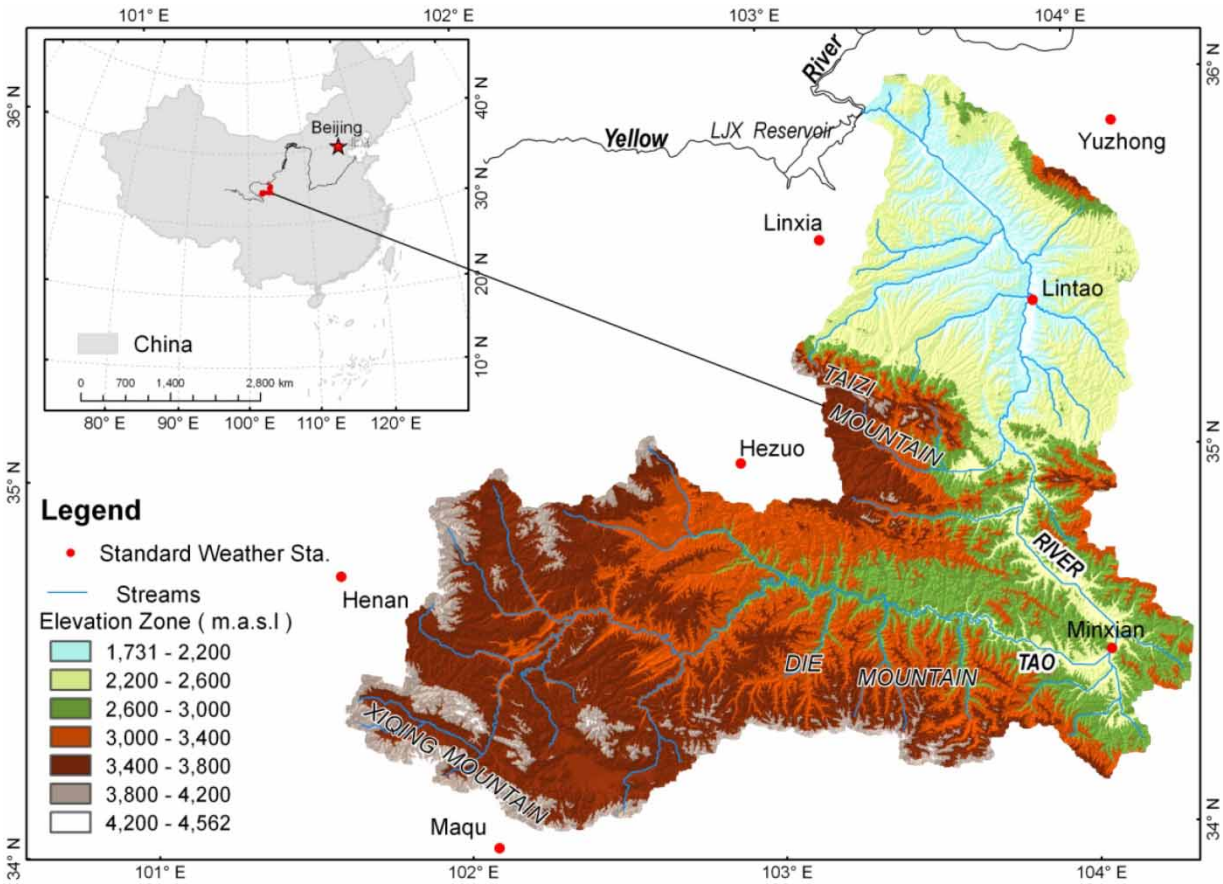

Figure 1 | Location of the TRB and the meteorological stations used in this study. The elevation zone was divided from 1,731 m to 4,562 m. The Taizi Mountain serves as a boundary to divide the TRB into two regions, the Gannan Plateau in the upper and middle stream and the Longxi Loess Plateau in the low stream region.

Table 1 | Geographic characteristics of the stations selected in this study

Stations	Longitude (dec. deg.)	Latitude (dec. deg.)	Elevation (m a.s.l)	T (°C)	PPT (mm/year)	ET_0 (mm/year)
Henan	101.60	34.73	1,350.0	0.23	561.7	627.7
Hezuo	102.90	35.00	2,910.6	2.84	527.7	665.9
Lintao	103.87	35.40	1,893.8	7.51	489.2	731.6
Linxia	103.18	35.58	1,917.2	7.33	489.9	715.9
Maqu	102.08	34.00	3,471.4	1.87	590.9	714.3
Minxian	104.07	34.47	2,315.0	6.14	556.2	665.9
Yuzhong	104.15	35.87	1,874.4	6.99	367.9	812.0

METHODOLOGY

Reference evapotranspiration (ET_0)

The daily reference evapotranspiration (ET_0) in the TRB was calculated using the P-M equation (Allen *et al.* 1998). The ET_0 represents a hypothetical crop that closely resembles the evaporation of an extensive surface of green grass that is actively growing and adequately watered with an assumed uniform height of 0.12 m, a surface resistance of 70 s/m, and an albedo of 0.23. The equation has been used to calculate daily reference evapotranspiration ET_0 (mm/d) for a wide range of locations and climates (Liang *et al.* 2008; Pirkner *et al.* 2013; Huo *et al.* 2013). The P-M equation is:

$$ET_0 = \frac{0.408\Delta(R_n - G) + \gamma(900/(T+273))U_2(e_s - e_a)}{\Delta + \gamma(1 + 0.34U_2)} \quad (1)$$

where ET_0 is the potential evapotranspiration or evapotranspiration capacity (mm), Δ is the slope of the saturation vapor pressure–temperature relationship (kPa/°C), R_n is the net radiation at the surface (MJ/m^2), G is the soil heat flux (MJ/m^2), T is the mean air temperature at a height of 2 m (°C), e_s represents the saturation vapor pressure (kPa), e_a represents the air vapor pressure (kPa), γ is the psychrometric constant (kPa/°C), and U_2 represents the average wind speed at a 2-m height above the surface over a 24-hour period (m/s).

The key radiation component of the P-M equation was estimated using the following procedures: in this study, we estimated the net radiation with a daily time scale as follows:

$$R_n = R_{ns} - R_{nl} \quad (2)$$

where R_{ns} is the incoming net shortwave radiation (MJ/m^2) and R_{nl} is the outgoing net longwave radiation (MJ/m^2). The incoming net shortwave radiation is estimated as the balance between the incoming and reflected solar radiation:

$$R_{ns} = (1 - \alpha)R_s \quad (3)$$

where α is the albedo (ranging from 0 to 1) and the solar radiation R_s is calculated using an empirical equation:

$$R_s = \left(a_s + b_s \frac{n}{N}\right)R_a \quad (4)$$

where a_s and b_s are the regression constants that are calibrated using the measured solar radiation data; in our study, we used the recommended values, i.e., $a_s = 0.25$ and $b_s = 0.5$ (Allen *et al.* 1998; Liu *et al.* 2010); n is the actual sunshine duration, N is the maximum possible sunshine duration, R_a is the extraterrestrial solar radiation (MJ/m^2). The net longwave outgoing radiation is calculated using the following equation:

$$R_{nl} = \sigma\left(\frac{(T_{min}+273.2)^4 + (T_{max}+273.2)^4}{2}\right)(0.34 - 0.14\sqrt{e_a})\left(1.35\frac{R_s}{R_{so}} - 0.35\right) \quad (5)$$

where σ is the Stefan–Boltzmann constant (4.903×10^9 MJ/(K^{4}m^{2}d)), T_{min} and T_{max} are the minimum and maximum air

temperatures (°C), respectively, and R_{so} is the clear-sky solar radiation (MJ/m^2).

Actual evapotranspiration (*AET*)

Observations of the annual terrestrial surface water balance demonstrate a tight and relatively simple functional dependence of evapotranspiration on the atmospheric water supply (precipitation) and demand (potential evaporation) at the surface (Lintner *et al.* 2015). Through dimensional analysis and mathematical reasoning, Fu added a parameter on the Budyko hypothesis to emphasize the influence of soil and landscape properties as (Fu 1981; Yang *et al.* 2006; Xu *et al.* 2013):

$$\frac{AET}{PPT} = 1 + \frac{ET_0}{PPT} - \left[1 + \left(\frac{ET_0}{PPT}\right)^{\varpi}\right]^{1/\varpi} \tag{6}$$

where AET is the actual evapotranspiration (mm), PPT is the precipitation (mm), ET_0 is the reference evapotranspiration (mm), and ϖ is a nondimensional constant of integration ranging from 0 to ∞. Yang *et al.* (2007) applied Fu's equation together with the parameter ϖ estimated by the empirical formula, have shown that Fu's equation can predict both long-term mean and annual value of actual evapotranspiration accurately and reasonably for 108 catchments including the Tibetan Plateau, Loess Plateau, Haihe River Basin, and inland river basins of China. We selected a value of 2.1 for ϖ based on Yang *et al.*'s (2007) study in TRB.

Statistical tests for trend analysis

Mann–Kendall trend test

The Mann–Kendall test, recommended by WMO, is also called Kendall's tau test according to Mann (1945) and Kendall (1975). This test is used to assess the significance of a trend based on a non-parametric test and is widely used in hydrometeorological trend detection studies. For a time-ordered sample of data x_i (i = 1, 2, … , n), x_i is independent and identically distributed. The test statistic S is given by:

$$\mathrm{S} = \sum_{i<j} a_{ij} \tag{7}$$

where

$$a_{ij} = sgn(x_j - x_i) = \begin{cases} 1 & x_i < x_j \\ 0 & x_i = x_j \\ -1 & x_i > x_j \end{cases} \tag{8}$$

As can be seen from Equation (8), the test statistic S only depends on the ranking of the observations, rather than their actual values, resulting in a distribution-free test statistic, which has the advantage that its power and significance are not affected by the actual distribution of the data (Khaled 2008). This is based on the assumption that the data are independent and identically distributed, with the mean and variance given by:

$$E(S) = 0 \tag{9}$$

$$Var(S) = n(n-1)(2n+5)/18 - \sum_{i=1}^{n} t_i(t_i-1)(2t_i+5)/18 \tag{10}$$

where t_i denotes the number of ties of extent i. The significance of the trends can be tested by comparing the standardized variable Z_c with the standard normal variable at the desired significance level α, given by:

$$Z_c = \begin{cases} \dfrac{S-1}{\sqrt{\mathrm{var}(s)}} & S > 0 \\ 0 & S = 0 \\ \dfrac{S+1}{\sqrt{\mathrm{var}(s)}} & S < 0 \end{cases} \tag{11}$$

where Z_c denotes the test statistics, when $|Z_c| > Z_{1-\alpha/2}$, in which $Z_{1-\alpha/2}$ are the standard normal deviates and α is the significance level for the test (Khaled & Rao 1998).

Sen slope

The change magnitudes of meteorological variables in this study were estimated using the Sen slope method. This method calculates the slope as a change in the measurement per change in time, with advantages of allowing missing data, there are no assumptions with respect to the distribution of the data, the data are not affected by gross data

errors or outliers (Sen 1968), and the impact of missing data or anomalous trends can be eliminated by using the median of the series of slopes as the judgmental basis. The expression is given by (Zuo *et al.* 2012):

$$\beta = Median\frac{(x_j - x_i)}{(j-i)},\ \forall j > i \tag{12}$$

where β is a robust estimation of the slope. A positive value of β indicates an 'increasing trend', and a negative value indicates a 'decreasing trend'. For a time series of annual values, β represents the annual increment under the hypothesis of a linear trend. This estimator provides the real slope of the tendency, which can differ slightly from the slope of the trend line obtained by linear regression (Espadafor *et al.* 2011).

Sensitivity analyses and their coefficients

For multi-variable models such as the P-M equation, different variables have different dimensions and ranges. Consequently, it is difficult to compare the sensitivity of each dependent variable with respect to ET_0 using partial derivatives. McCuen (1974) and Beven (1979) recommended a mathematical definition equation of a sensitivity coefficient to describe the sensitivity characteristics with a non-dimensional form, which is widely used in evapotranspiration studies (Gong *et al.* 2006; Liu and Luo 2010; Huo *et al.* 2013):

$$S_{v_i} = \lim_{\Delta Vi \to 0}\left(\frac{\Delta ET_0/ET_0}{\Delta V_i/V_i}\right) = \frac{\partial ET_0}{\partial V_i}\cdot\frac{V_i}{ET_0} \tag{13}$$

where S_{vi} is the sensitivity coefficient of the ith variable (V_i). A positive or negative sensitivity coefficient indicates that the ET_0 will increase or decrease, respectively, with increases in the given variable. The larger the coefficient of a variable, the more sensitive the ET_0 to the variable, i.e., the larger the impact the given variable has on ET_0. In theory, the coefficient is the tangent slope of the sensitivity curve. In practice, however, the coefficient is represented by a given 'linear range' around the origin. If the sensitivity curve is linear, the coefficient remains constant regardless of any perturbation in the variable concerned; if the sensitivity curve is non-linear, the coefficient will change with the perturbation of the respective variable, which depends on the degree of non-linearity of the curve. The smaller the variable perturbation, the more accuracy of the coefficient (Liu *et al.* 2010).

The procedure used to detect the factors influencing the ET_0 trends and to execute the quantitative evaluation is as follows: ET_0 was recalculated by making a ±10% change in each meteorological factor (R_n, T_{max}, T_{min}, Rh, U_2) assuming other factors were fixed; the sensitivity coefficient (S_v) was calculated from Equation (13); and the ET_0 change induced by one variable was indicated by multiplying the relative change of the variable by its S_v (Yin *et al.* 2010). For example, a sensitivity coefficient of 0.2 for a given variable means that when the variable increases by 10%, all other variables remain constant, but the ET_0 may increase by 2%. In our study, sensitivity coefficients were estimated based on a daily time series. Yearly average sensitivity coefficients were obtained by averaging the daily values.

Quantifying the influence of changes in climate variables

The method to estimate the contributions of key climate variables to the change trends of reference and actual evapotranspiration is similar to Xu *et al.* (2006). The steps include three parts, as follows. (1) Converting the temperature, wind speed, humidity, and solar net radiation into a stationary time series by removing their change trends using the detrend equation (Huo *et al.* 2013):

$$V_{detrend,i} = V_{original,i} - S \times i \quad (i = 1, 2, \ldots N) \tag{14}$$

where $V_{detrend,i}$ is detrended variable series, $V_{original,i}$ is the original series, S is the change trend of the given variable, i is the number of times, and N is the length of variable time series. (2) Recalculating the evapotranspiration (ET_0 or AET) using only one detrended climate factor data series and using the original data for the other climate variables. (3) Contrasting the recalculated evapotranspiration with the original value. The difference is considered to be due to the climate variable impact on reference evapotranspiration.

RESULTS AND DISCUSSION

Validating the calculated ET_0 and *AET*

Based on the observed pan evaporation from 1987 to 2005 at the Minxian meteorological station, we validated the value calculated by the P-M method. A comparison between observed pan evaporation and P-M ET_0 is presented in Figure 2. P-M ET_0 is consistent with the corresponding value of pan evaporation and the correlation coefficient is 0.96, which indicates that the calculated evapotranspiration based on the P-M equation is reliable and can represent the real condition of TRB.

Due to a lack of eddy covariance or other available measured actual evapotranspiration data in our study area, we used the evapotranspirable water estimated by *PPT-R* (precipitation minus runoff) to validate the *AET* calculated by Fu's equation. The evapotranspirable water and the results simulated using Fu's equation is presented in Figure 3, for which the correlation coefficient is 0.73 and the Nash–Sutcliffe efficiency is 0.66 for the whole TRB. The respective correlation and Nash–Sutcliffe efficiency coefficients are 0.78 and 0.62 for the Ganan Plateau and 0.64 and 0.81 for the Loess Plateau. For high *PPT-R* values, the simulated *AET* was underestimated based on a comparison with the evapotranspirable water and the corresponding points plotted above the 1:1 line in the scatterplots, especially in the Gannan Plateau. For low *PPT-R* values, the *AET* was mainly overestimated based on the evapotranspirable water and the corresponding points plotted below the 1:1 line in the scatterplot, especially in the Loess Plateau. According to the results of the field investigation, not all of the evapotranspirable water was consumed by evapotranspiration and some was partially stored in the soil as soil water. The difference from estimated *AET* to *PPT-R* reflects the reservoir function of the underlying soil. Generally, at a higher *PPT-R*, relatively more water is stored in the soil. The precipitation is heavy with low intensity, water is intercepted by the canopy and some stored in the soil pore as soil water, little water flows out as runoff, which leads to the estimated *AET* smaller than *PPT-R*. Therefore, the underestimated *AET* in the Gannan Plateau is reasonable, especially in 2003. The *AET* was overestimated in the Loess Plateau mainly due to the evapotranspirable water (*PPT-R*) and soil water was consumed by vegetation evapotranspiration through capillary action and root hydraulic lift

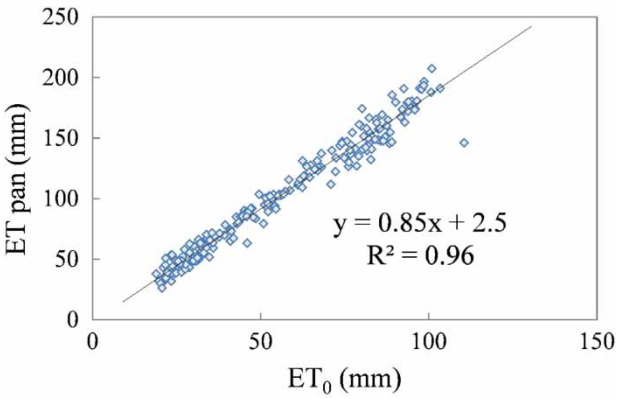

Figure 2 | The correlation between the value of *ET* based on pan evaporation and the P-M equation, using the Minxian meteorological station as an example.

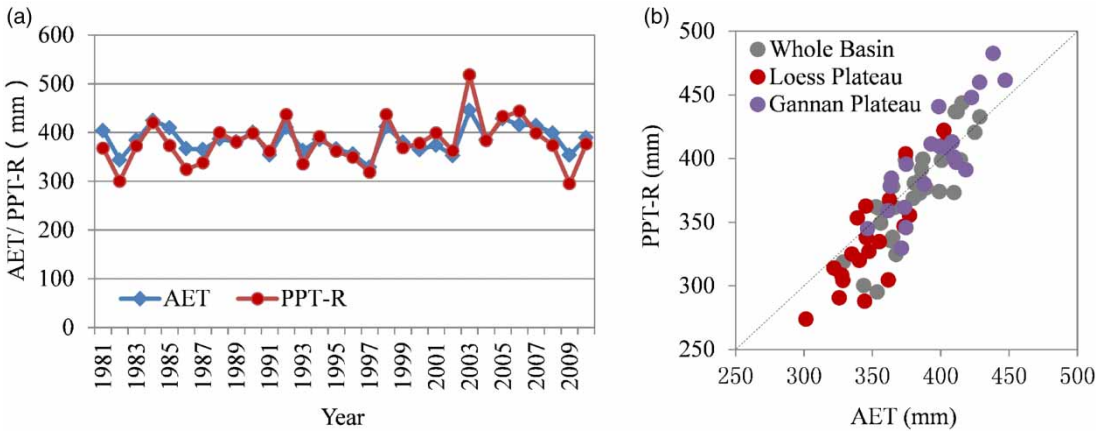

Figure 3 | Comparison of annual *AET* and *PPT-R* values: (a) time series contrast (1981–2010), (b) scatterplots between *PPT-R* and *AET*.

in order to meet the needs of evapotranspiration ability, which leads to the estimated *AET* being larger than *PPT-R*. This is consistent with the characteristics of the hydrological cycle in this area, such as in 2009. Overall, statistics show that the average annual *PPT-R* was 396 mm and the estimated *AET* was 381 mm in the TRB. The relative error is therefore approximately 1.77%. This indicates that the performance results were within the acceptable bounds and the simulated series are stable and reliable without systematic error, which means the method of estimating *AET* using Fu's equation based on the Budyko hypothesis was suitable for the TRB. We used Fu's equation to estimate the *AET* and its spatial and temporal variability in the TRB.

Changes in climate variable trends

We further divided the annual data into four seasons: winter (December to February), spring (March to May), summer (June to August), and autumn (September to November) for seasonal analyses. In this way, we detected the variability of meteorological variables in different seasons. The seasonal trends and magnitudes of several key climatic variables from 1981 to 2010 are summarized in Table 2. Considerable changes occurred due to climate variability in both the GPA and the LPA. In the past 30 years, the trend of maximum air temperature (T_{max}) and minimum air temperature (T_{min}) increased with significant magnitude in the four seasons. The increase in T_{max} and T_{min} is much more evident in the cooler than in the warmer seasons in the two plateau areas. The greatest rate of increase in T_{max} and T_{min} happened in winter at 0.083 and 0.077 °C per year ($P < 0.01$) in GPA and 0.084 and 0.061 °C per year ($P < 0.01$) in LPA, respectively. Net solar radiation (R_n) and wind speed (U_2) increased with different levels of significance during the four seasons in the GPA and LPA, except for the decreasing trend of R_n in autumn in the LPA. Relative humidity (*Rh*) and precipitation (*PPT*) decreased in the GPA in all the seasons except autumn; in LPA, *Rh* decreased in spring and summer and *PPT* decreased in all seasons except autumn, with different levels of significance.

It was noted that annual T_{max} and T_{min} significantly increased in the GPA by 0.066 and 0.054 °C per year, which is higher than in the LPA, i.e., 0.063 and 0.024 °C per year ($P < 0.01$), respectively. R_n significantly increased by 3.66 MJ/m^2 per year ($P < 0.05$) in the GPA and 2.01 MJ/m^2 per year ($P < 0.1$) in the LPA. The decreasing trends of *Rh* in the GPA and increasing trends of U_2 in the LPA were also remarkable during the last 30 years.

The increase in R_n and air temperature and decrease in *Rh* led to an increase in ET_0. The IPCC (2014) reported an increase in global average surface temperature of approximately 0.85 °C from 1880 to 2012, which very likely has resulted from the increase in human-induced emission of greenhouse gases. Our study showed a remarkable increase in air temperature, which is consistent with other studies in semi-arid and semi-humid regions of China. Although the annual *PPT* decreased without significance, it had an important influence on evapotranspiration in this water-limited region. Solar radiation is the fundamental energy source on Earth. Long-term records of surface radiation measurements suggest that surface solar radiation increased in TRB. It was quite different to other studies that surface solar radiation decreased in many regions during this period (Xu *et al.* 2006; Liu *et al.* 2010; Peng *et al.* 2013). It is called 'From Dimming to Brightening'. The changes in cloud cover, aerosol emissions, and air pollution associated with economic developments are widely considered to be responsible for a substantial part of 'From Dimming to Brightening' (Cheng *et al.* 2013; Matin & Bourque 2013). Different change trends and magnitudes of climatic variables have been reported for different eco-geographical regions around the world (Liang *et al.* 2008; Pirkner *et al.* 2013; Huo *et al.* 2013).

Changes in the ET_0 and *AET* trends

The distribution of ET_0 was interpolated using station-based ET_0 and a kriging method in the TRB (Figure 4). As the kriging method has the highest correlation coefficient calculated from the cross-validation test (Liu *et al.* 2010), it was selected for interpolating yearly ET_0 and *AET* in this study. The annual average ET_0 of the TRB is 691 mm. From the upstream to downstream regions, the ET_0 gradually increased, ranging from 633 mm to 789 mm. The ET_0 in the downstream region of the LPA was generally higher than in the upstream region of the GPA, i.e., 743 mm versus 673 mm. The Sen slope statistics showed an increasing annual ET_0 trend in the TRB, at a rate of 3.43 mm per

Table 2 | Trend analysis results of climate variables based on Sen slope and the M-K test

		GPA			LPA		
Seasons	**Variables**	**Z**	**β**	**Signific.**	**Z**	**β**	**Signific.**
Spring	*Rn* (MJ/m^2)	1.78	1.199	+	1.46	0.944	
	T_{max} (°C)	3.71	0.080	**	3.53	0.087	**
	T_{min} (°C)	3.50	0.041	**	3.28	0.048	**
	Rh (%)	−3.00	−0.002	**	−2.00	−0.002	*
	U_2 (m/s)	0.50	0.002		1.32	0.007	
	PPT (mm)	−1.28	−0.658		0.50	0.183	
Summer		1.32	1.143		1.50	1.399	
		3.07	0.050	**	3.18	0.070	
		3.57	0.065	**	3.43	0.054	
	Rh (%)	−2.78	−0.001	**	−2.18	−0.002	*
	U_2 (m/s)	1.36	0.005		2.82	0.015	**
	PPT (mm)	−0.57	−0.802		−1.14	−1.460	
Autumn		1.89	0.762	+	−0.21	−0.138	
		3.35	0.064	**	2.25	0.053	*
		2.25	0.044	*	1.86	0.024	+
	Rh (%)	−0.46	0.000		1.36	0.001	
	U_2 (m/s)	1.25	0.004		2.46	0.010	*
	PPT (mm)	0.29	0.343		−0.04	−0.079	
Winter		0.88	0.146		0.13	0.042	
		2.68	0.083	**	2.76	0.084	**
		3.47	0.077	**	3.10	0.061	**
	Rh (%)	−0.51	−0.001		−0.13	0.000	
	U_2 (m/s)	1.29	0.007		2.04	0.011	*
	PPT (mm)	−0.62	−0.099		−1.29	−0.138	
Annual		2.36	3.661	*	1.89	2.014	+
		4.28	0.066	**	3.71	0.063	**
		4.17	0.054	**	4.25	0.043	**
	Rh (%)	−2.11	−0.001	*	−1.21	−0.001	
	U_2 (m/s)	1.00	0.005		1.82	0.010	+
	PPT (mm)	−0.68	−1.308		−0.93	−1.465	

Note: Positive values in the table indicate an increase and negative values indicate a decrease.
+ Indicates a significance level of 0.1.
*Indicates a significance level of 0.05.
**Indicates a significance level of 0.01.

year over the 30 years from 1981 to 2010. Compared with the increased magnitudes in the downstream region of the LPA, the magnitude in the upstream region of the GPA is slightly lower. The former is 3.54 mm per year, and the latter is 3.39 mm per year.

The *AET* was calculated using Fu's equation and combining the interpolated ET_0 and precipitation. The distribution of annual *AET* showed distinct spatial heterogeneity in the two regions. The annual *AET* in the Gannan and LPAs was 398 mm and 345 mm, respectively. The

highest *AET* occurred in the south, and the lowest value occurred in the north of the TRB. The *AET* in the GPA is higher than in the LPA, where the water is limited. The results from the Sen slope statistics suggested a slight increasing trend with a moderate magnitude occurred in the GPA, while in the LPA the *AET* changed at a considerable rate and a unique decrease occurred in this region. The annual *AET* trend change in the Gannan Plateau increased by 0.54 mm per year compared with a decrease of 0.06 mm per year in the LPA.

Based on the ET_0 and *AET* analyses, we found that ET_0 and *AET* increased in the semi-humid GPA, while in the semi-arid region of the LPA ET_0 increased and *AET* decreased over the last 30 years. This is consistent with recent studies (Yang *et al.* 2006, 2007). In humid and semi-humid regions, changes in *AET* are dominated by changes in potential evapotranspiration based on the Penman hypothesis rather than precipitation. However, in arid and semi-arid regions, changes in *AET* are dominated by changes in precipitation rather than ET_0. *AET* and ET_0 are correlated by a complementary relationship via precipitation. In this study, the underlying climate factors causing the changes in ET_0 and *AET* in the whole basin are discussed in the following sections.

Sensitivity analysis of ET_0 and *AET*

Application of the Beven method resulted in obvious differences of ET_0 sensitivity to climatic factors. The spatial distribution of annual ET_0 sensitivity coefficients to five key climate variables is shown in Figure 5. The sensitivity coefficients of ET_0 to net solar radiation varied from 0.66 to 0.77 and were higher in the midstream than in the up- and downstream regions of the TRB. However, the average

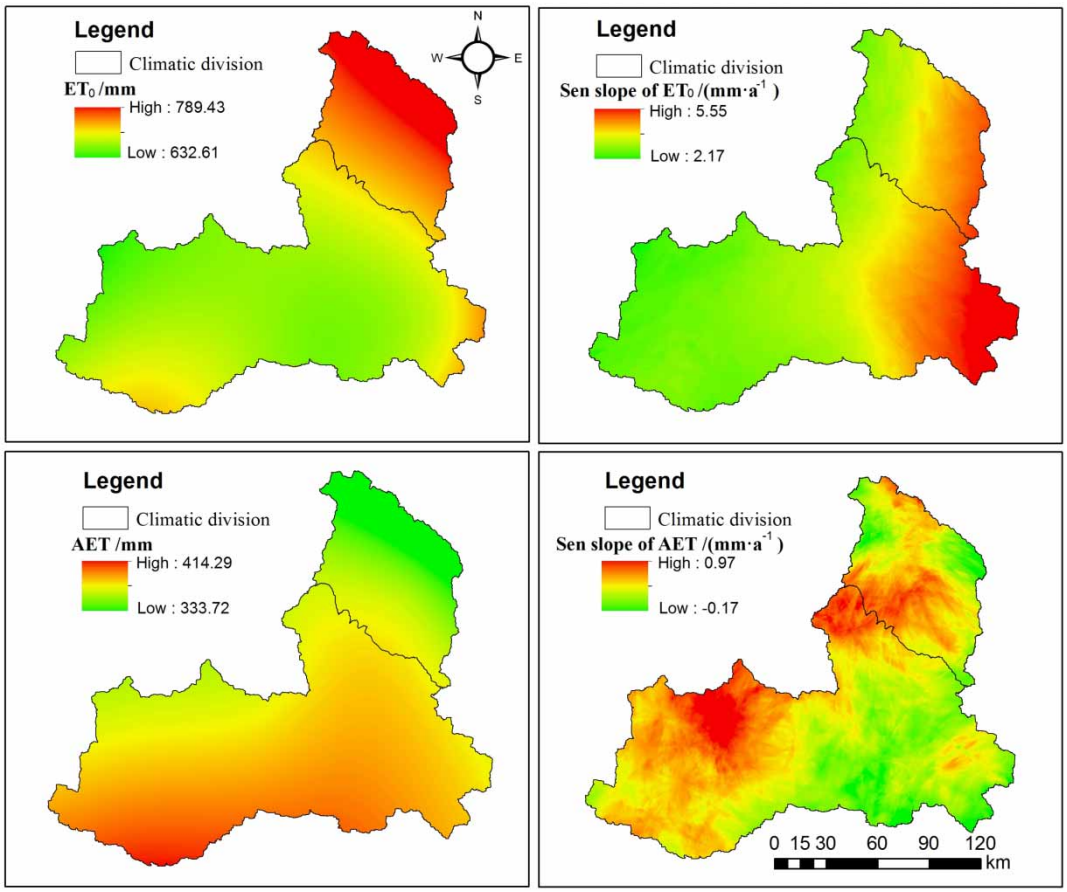

Figure 4 | Spatial distribution of average annual ET_0 and *AET* and their Sen slopes.

values of sensitivity coefficients of ET_0 to R_n in the GPA and LPA were the same, i.e., 0.73. The variability in the spatial distribution of the ET_0 sensitivity coefficients to maximum and minimum air temperature was similar. The sensitivity coefficients increased from the upstream to the downstream regions. The average sensitivity coefficients of ET_0 to T_{max} in the GPA and LPA were 0.30 and 0.32, respectively. The sensitivity coefficient of T_{min} was the same in the two plateaus, i.e., 0.26. The Rh coefficients varied from −0.62 to −0.47, with an average of −0.56 in the GPA and −0.52 in the LPA. The U_2 coefficient in the GPA was larger than that in the LPA, i.e., 0.14 and 0.11, respectively. Based on the above analysis, we found that the R_n, T_{max}, T_{min}, and U_2 coefficients were positive but the Rh coefficient was negative, which indicates that ET_0 will increase with increases in R_n, T_{max}, T_{min}, and U_2 and a decrease in Rh. Despite the different influences on ET_0, we ordered the sensitivity based on the absolute coefficients as follows: net solar radiation > relative humidity > maximum air temperature > minimum air temperature > wind speed for the entire TRB.

The spatial distribution of the annual AET sensitivity coefficients of six key climate variables is shown in Figure 6. The sensitivity coefficients of R_n varied from 0.34 to 0.19, with an average value of 0.31 in the GPA, which was higher than in the LPA, i.e., 0.23. Rh had a negative effect on AET, with negative sensitivity coefficients ranging from −0.13 to −0.27. The negative effect of Rh in the GPA was more significant with an absolute higher value of 0.23 compared with 0.15 in LPA. T_{max} and T_{min} had a similar effect on AET, with a similar spatial distribution of sensitivity coefficients ranging from 0.12 to 0.07. U_2 had a small sensitivity coefficient, which means the lowest influence on AET. In contrast, PPT had the greatest influence on AET with the largest sensitivity coefficients ranging from 2.82 to 3.67; the average value for the LPA was 3.41 compared with 2.92 for the GPA. This means that the influence of PPT on AET

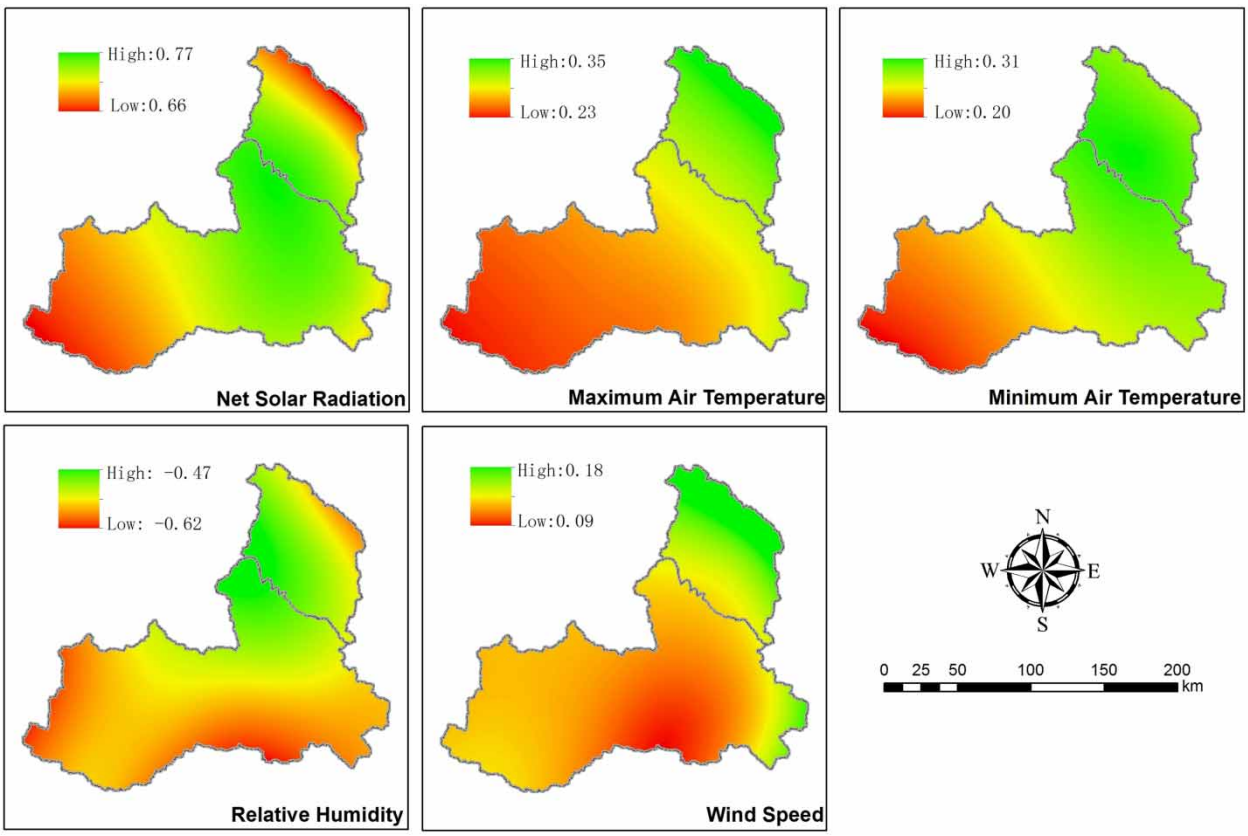

Figure 5 | Spatial distribution of ET_0 sensitivity coefficients for meteorological variables.

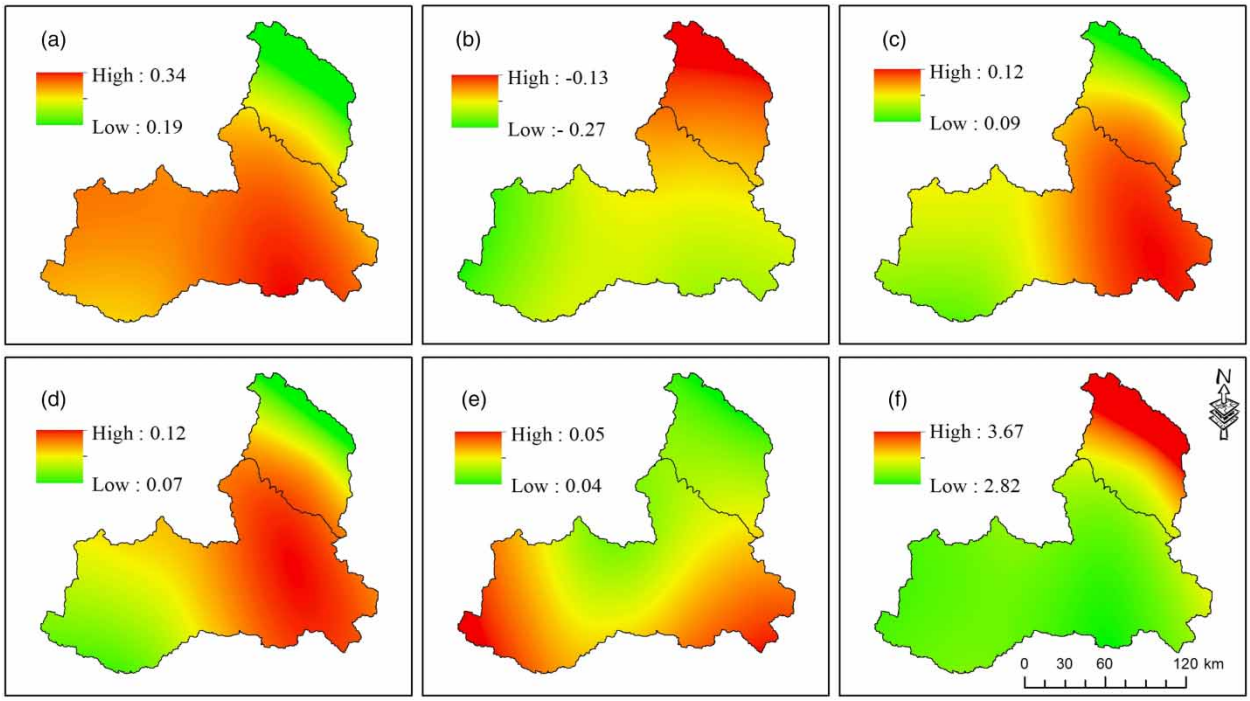

Figure 6 | Spatial distribution of *AET* sensitivity coefficients for meteorological variables: (a) net solar radiation, (b) relative humidity, (c) maximum air temperature, (d) minimum air temperature, (e) wind speed, (f) precipitation.

was more significant in the semi-arid region than in the sub-humid region. The sensitivity ranking of the climate factors to *AET* was precipitation > net solar radiation > relative humidity > maximum air temperature > minimum air temperature > wind speed in the entire TRB.

The sensitivity of ET_0 and *AET* to meteorological variables varies with climate characteristics in different regions. Huo *et al.* (2013) suggested that ET_0 is most sensitive to wind speed in arid regions of China, while Gong *et al.* (2006) concluded that relative humidity had the greatest influence on ET_0 in the humid Yangtze River Basin of China. However, in our study, we found that net solar radiation and relative humidity were the most sensitive ET_0 variables in the TRB with a semi-arid and semi-humid climate, which is consistent with the conclusion of Liu *et al.* (2010). The greater impact of relative humidity compared with wind speed on ET_0 is in agreement with the results presented by Zuo *et al.* (2012) for a semi-arid region. A comparison of the sensitivity of *AET* to meteorological factors indicated that precipitation is the most sensitive factor, and this variable had a higher coefficient in the LPA compared with GPA. This is consistent with the Budyko hypothesis that *AET* is controlled by *PPT* rather than ET_0 in water-limited regions (Liu *et al.* 2010).

Influence of climate variability on ET_0 and *AET*

In order to detect the response of ET_0 and *AET* to climate variability, it is necessary to detrend the climate variables. The original and detrended data series for every variable for the TRB is shown in Figure 7. Distinct differences can be observed between the original and detrended data series for the six meteorological factors. Net solar radiation, maximum and minimum air temperature, and wind speed exhibited positive trends, while relative humidity and precipitation exhibited negative trends. Consequently, the detrended data series of R_n, T_{max}, T_{min}, and U_2 were lower than the original, and the detrended data of *Rh* and *PPT* were larger than the original series. In general, climate variability contributed to increases in R_n, T_{max}, T_{min}, and U_2, with rates of 1.48%, 8.58%, 43.87%, and 11.61%, and decreases in *Rh* and *PPT*, with rates of −1.88% and −2.69%, respectively, during the past 30 years in the TRB.

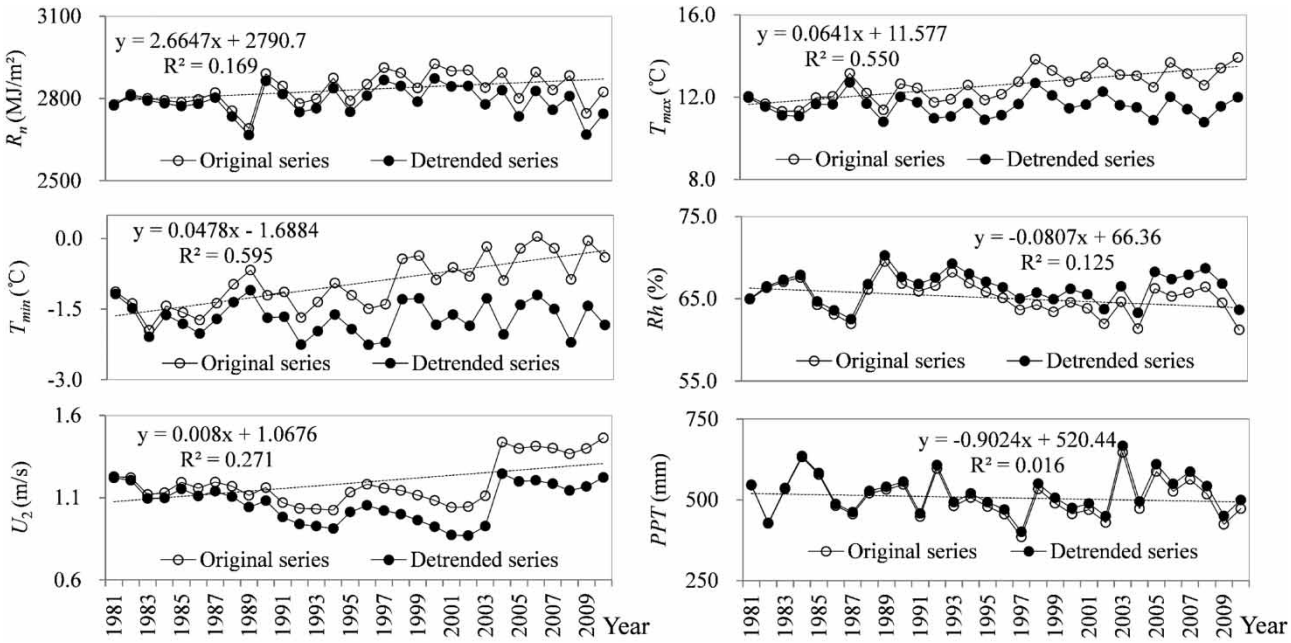

Figure 7 | Original and detrended series of *Rn*, T_{max}, T_{min}, *Rh*, U_2, and *PPT* from 1981 to 2010 in the entire TRB. Linear fitted trends of the original series are presented for the meteorological variables.

Using the detrended meteorological data series, the P-M equation and Fu's equation were used to recalculate the detrended ET_0 and *AET*. The contrast between the detrended and original value in the two plateaus is shown in Figure 8. Considerable changes in ET_0 occurred due to climate variability in the GPA and LPA, with increased rates of 6.47% and 6.10%, respectively, from 1981 to 2010. However, the changes in *AET* were not as obvious. The *AET* in the GPA increased at a rate of 1.33% but decreased in LPA at a rate of 0.93%. The distribution of the contribution of climate variability to ET_0 and *AET* is presented in Figure 9. The contribution of climate variability to ET_0 ranged from 2.54% to 13.43% with a high percentage in the eastern region of the TRB. The contribution of climate variability to *AET* varied from −2.05% to 2.48% with a low percentage in the eastern region of the TRB over the past 30 years.

The contribution of meteorological variables to changes in ET_0 and *AET* was determined based on the relationship between the sensitivity and the meteorological variables (Equation (13)). We can understand the independent influence of every meteorological factor on ET_0 and *AET*. Calculations showed that given the same increasing amplitude (+1%) of net solar radiation, relative humidity, maximum air temperature, minimum air temperature and wind speed, the relative increment of ET_0 due to sensitivity was 0.73%, −0.54%, 0.31%, 0.26%, and 0.13%, respectively. Over the past 30 years, changes in net solar radiation (1.48%) contributed to the ET_0 increase by 1.08%, decrease in relative humidity (−1.88%) contributed to increase in ET_0 by 1.01%, increase in maximum air temperature (8.58%) and minimum air temperature (48.37%) contributed to increase in ET_0 by 2.66% and 12.58%, respectively, and wind speed (11.61%) contributed to an ET_0 increase of approximately 1.5%. Despite the fact that the interaction within these variables contributed to the increase in ET_0, the increase in air temperature leading to the increase in ET_0 was obviously larger than other factors in the whole basin. Although ET_0 was more sensitive to R_n than to other factors, the changes in solar radiation were not the dominant factors for the changes in ET_0 in the TRB. The significant increases in air temperature were the dominant factor in the increase, because this was not only a relatively sensitive variable, but also exhibited a significant increasing magnitude over the 30 years.

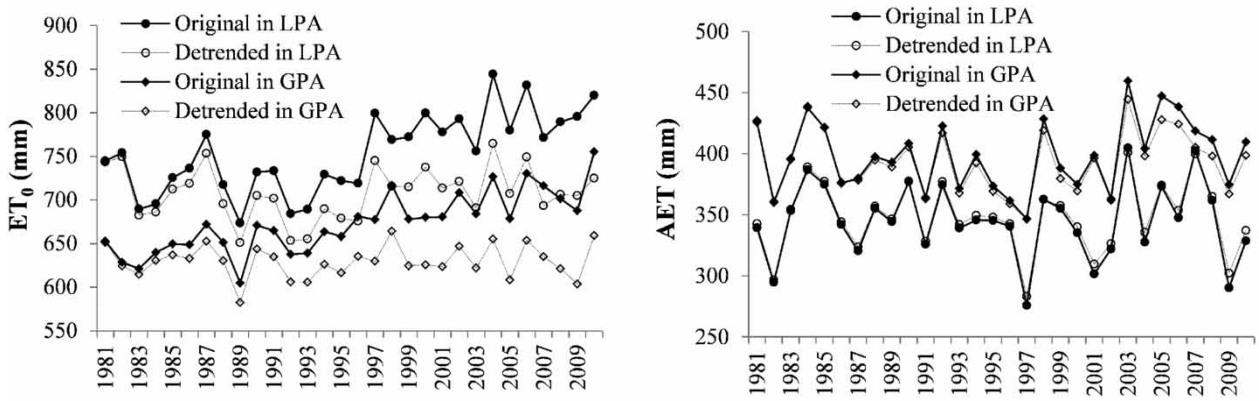

Figure 8 | Comparison of the original mean annual ET_0 and AET and the recalculated values with detrended variables in the two plateaus.

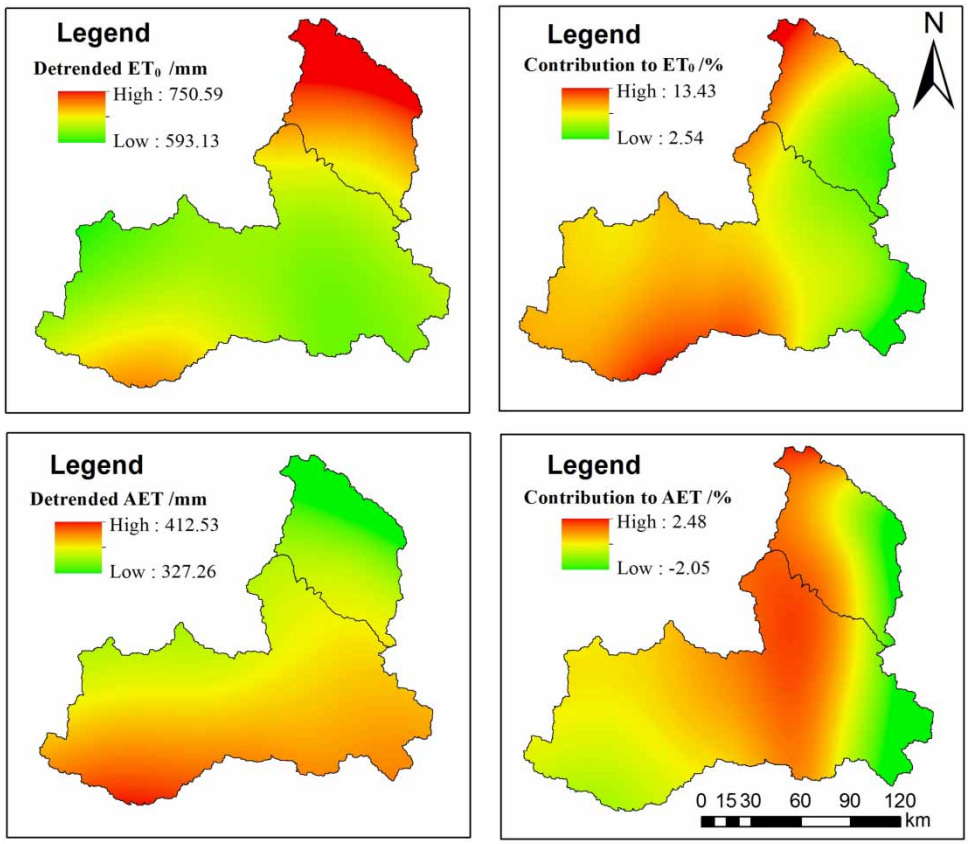

Figure 9 | Spatial distribution of detrended annual ET_0 and AET and their percentage contributions to climate variability.

The changes in AET resulted from climate variability, based on Fu's equation, mainly from the changes in precipitation and reference evapotranspiration. We detected the influences of climate variability on AET, similar to the analysis used to determine the influence on ET_0. With the same precipitation amplitude (+1%), the relative increment in AET was 2.92% in the GPA and 3.41% in LPA due to the sensitivity analysis. From 1981 to 2010, precipitation decreased in the GPA and LPA with amplitudes of −2.82% and −3.22%, which led to AET decreases of

8.23% and −10.98% in the two regions, respectively. However, we confirmed the *AET* exhibited an increasing trend in the GPA and a decreasing trend in LPA by Sen slope method. This indicated that the increase in *AET* resulting from the increase in ET_0 completely offset the decrease in *AET* resulting from the decrease in *PPT*, which subsequently resulted in an increase in *AET* in GPA. While, in LPA, the increase in *AET* resulting from the increase in ET_0 did not completely offset the decrease in *AET* resulting from the decrease in *PPT*, and subsequently resulted in a decrease in *AET*. Combining with the analyses of climate factors impacts on ET_0, *AET* was controlled by air temperature rather than precipitation in the semi-humid GPA region based on the Penman hypothesis, but was controlled by precipitation rather than ET_0 in the semi-arid LPA region based on the complementary hypothesis.

CONCLUSIONS

Analysis of the impact of climate variability on evapotranspiration is of great importance to eliminate threats and manage the water budget for agricultural purposes. In this study, temporal and spatial variations in ET_0 and *AET* were comprehensively detected. The spatial distributions of the annual sensitivity of ET_0 and *AET* to key climate variables were investigated. The quantitative contributions of the major meteorological variables to ET_0 and *AET* were evaluated and the dominant controlling factors were also analyzed in the TRB from 1981 to 2010. The following conclusions can be drawn from this study.

Considerable increase in ET_0 occurred in the GPA and LPA, by 6.47% and 6.10%, respectively. The *AET* increased in the GPA by 1.33% but decreased in the LPA by 0.93% from 1981 to 2010. The spatial distribution of the sensitivity of ET_0 and *AET* to the same climatic variables showed significant differences among locations. The greatest impact of climate factor on ET_0 was net solar radiation followed by relative humidity, maximum and minimum air temperature, and wind speed. The increase in ET_0 was mainly caused by the significant increase in air temperature across the entire TRB, which contributed to the increase in ET_0 by approximately 7.62%. Precipitation was the most sensitive factor for *AET* followed by net solar radiation, relative humidity, maximum and minimum air temperature, and wind speed. The decrease in *PPT* was responsible for the decrease in *AET* in the LPA, which contributed to the decrease in *AET* by 10.98%, while the effect of ET_0 on *AET* offset the effect of *PPT* on *AET* in the GPA, which resulted in an increasing *AET* due to the increase in ET_0. The results indicated the dominant controlling factor on *AET* is air temperature in the GPA based on the Penman hypothesis and in the LPA is *PPT* based on the complementary hypothesis.

In addition, the climate factors (R_n, T_{max}, T_{min}, U_2, *Rh*, and *PPT*) considered in this study should be independent of each other to ensure each factor is represented by its individual contribution. Uncertainties existed in the estimation of the contributions of climate variables. The errors could come from the assumption that the six climate variables were independent in the differential detrend processes. However, the six climate variables impact each other and are not totally independent, leading to uncertainties and errors.

ACKNOWLEDGEMENTS

This study was supported by the National Natural Science Foundation of China (31370466), the China Postdoctoral Science Foundation (2015M572620). The authors would like to thank the editors and anonymous reviewers for their detailed and constructive comments, which helped to significantly improve the manuscript.

REFERENCES

Allen, R. G., Pereira, L. S., Raes, D. & Smith, M. 1998 *Crop Evapotranspiration Guidelines for Computing Crop Water Requirements*. FAO Irrigation and Drainage Paper 56, Rome, Italy.

Beven, K. 1979 A sensitivity analysis of the Penman-Monteith actual evapotranspiration estimates. *J. Hydrol.* **44**, 169–190.

Brutsaert, W. 2013 Use of pan evaporation to estimate terrestrial evaporation trends: the case of the Tibetan Plateau. *Water Resour. Res.* **49**, 3054–3058.

Budyko, M. I. 1961 The heat and water balance of the Earth's surface, the general theory of physical geography and the problem of the transformation of nature. *Sov. Geogr.* **2**, 3–12.

Budyko, M. I. 1974 *Climate and Life* (D. H. Miller Trans.). Academic Press, San Diego, CA, USA.

Cheng, D. H., Li, Y., Chen, X., Wang, W., Hou, G. & Wang, C. 2013 Estimation of groundwater evaportranspiration using diurnal water table fluctuations in the Mu Us Desert, northern China. *J. Hydrol.* **490**, 106–113.

Espadafor, M., Lorite, I. J., Gavilán, P. & Berengena, J. 2011 An analysis of the tendency of reference evapotranspiration estimates and other climate variables during the last 45 years in Southern Spain. *Agric. Water Manage.* **98** (6), 1045–1061.

Fu, B. P. 1981 On the calculation of the evaporation from land surface. *Sci. Atmos. Sin.* **5** (1), 23–31 (in Chinese).

Gong, L., Xu, C., Chen, D., Halldin, S. & Chen, D. 2006 Sensitivity of the Penman-Monteith Reference evapotranspiration to key climatic variables in the Changjiang (Yangtze River) basin. *J. Hydrol.* **329** (3/4), 620–629.

Goyal, R. K. 2004 Sensitivity of evapotranspiration to global warming: a case study of arid zone of Rajasthan India. *Agric. Water Manage.* **69** (1), 1–11.

Huo, Z., Dai, X., Feng, S., Kang, S. & Huang, G. 2013 Effect of climate variability on reference evapotranspiration and aridity index in arid region of China. *J. Hydrol.* **492**, 24–34.

IPCC 2014 *Climate Change 2014: Synthesis Report. Contribution of Working Groups I, II and III to the Fifth Assessment Report of the Intergovernmental Panel on Climate Change* (Core Writing Team, R. K. Pachauri and L. A. Meyer, eds). IPCC, Geneva, Switzerland, 151 pp.

Jiang, C., Xiong, L., Wang, D., Liu, P., Guo, S. & Xu, C. Y. 2015 Separating the impacts of climate variability and human activities on runoff using the Budyko-type equations with time-varying parameters. *J. Hydrol.* **522**, 326–338.

Jung, M., Reichstein, M., Ciais, P., Seneviratne, S. I., Sheffield, J., Goulden, M. L. & Zhang, K. 2010 Recent decline in the global land evapotranspiration trend due to limited moisture supply. *Nature* **467** (7318), 951–954.

Katul, G. G., Oren, R., Manzoni, S., Higgins, C. & Parlange, M. B. 2012 Evapotranspiration: A process driving mass transport and energy exchange in the soil-plant-atmosphere-climate system. *Rev. Geophys.* **50**, RG3002.

Kendall, M. G. 1975 *Rank Correlation Methods*. Griffin, London, UK.

Khaled, H. 2008 Trend detection in hydrologic data: The Mann-Kendall trend test under the scalling hypothesis. *J. Hydrol.* **349**, 350–363.

Khaled, H. & Rao, A. R. 1998 A modified Mann-Kendall trend test for autocorrelated data. *J. Hydrol.* **204**, 182–196.

Kite, G. 2000 Using a basin-scale hydrological model to estimate crop transpiration and soil evaporation. *J. Hydrol.* **229**, 59–69.

Li, C. B., Qi, J. G., Yang, L. S., Wang, S. B., Yang, W. J., Zhu, G. F., Zou, S. B. & Zhang, F. 2014 Regional vegetation dynamics and its response to climate variability – a case study in the Tao River Basin in Northwestern China. *Environ. Res. Lett.* **9** (12). doi:10.1088/1748-9326/9/12/125003.

Li, C. B., Zhang, X. L., Qi, J. G., Wang, S. B., Yang, L. S., Yang, W. J., Zhu, G. F. & Hao, Q. 2015 A case study of regional eco-hydrological characteristics in the Tao River Basin, northwestern China, based on evapotranspiration estimated by a coupled Budyko Equation-crop coefficient approach. *Sci. Chin. Ser. D-Earth Sci.* **58**, 2103–2112.

Liang, L., Li, L., Zhang, L., Li, J. & Li, B. 2008 Sensitivity of Penman-Monteith reference crop evapotranspiration in Tao'er River Basin of Northeastern China. *Chin. Geogr. Sci.* **18** (4), 340–347.

Lintner, B. R., Gentine, P., Findell, K. L. & Salvucci, G. D. 2015 The Budyko and complementary relationships in an idealized model of large-scale land–atmosphere coupling. *Hydrol. Earth Syst. Sci.* **19**, 2119–2131.

Liu, Y. & Luo, Y. 2010 A consolidated evaluation of the FAO-56 dual crop coefficient approach using the lysimeter data in the North China Plain. *Agr. Water Manage.* **97**, 31–40.

Liu, Q., Yang, Z., Cui, B. & Sun, T. 2010 The temporal trends of reference evapotranspiration and its sensitivity to key meteorological variables in the Yellow River Basin, China. *Hydrol. Process.* **24** (15), 2171–2181.

Mackay, D. S., Frank, J., Reed, D., Whitehouse, F., Ewers, B. E., Pendall, E. & Sperry, J. S. 2012 Modeling evapotranspiration based on plant hydraulic theory can predict spatial variability across an elevation gradient and link to biogeochemical fluxes. *EGU General Assembly Conference Abstracts* **14**, 11461.

Mann, H. B. 1945 Nonparametric tests against trend. *Econometrica* **13**, 245–259.

Matin, M. A. & Bourque, C. 2013 Assessing spatiotemporal variation in actual evapotranspiration for semi-arid watersheds in northwest China: evaluation of two complementary-based methods. *J. Hydrol.* **486**, 455–465.

McCuen, R. H. 1974 A sensitivity and error analysis of procedures used for estimating evapotranspiration. *Water Res. Bull.* **10** (3), 486–498.

Peng, J., Liu, Y., Zhao, X. & Loew, A. 2013 Estimation of evapotranspiration from MODIS TOA radiances in the Poyang Lake basin, China. *Hydrol. Earth Syst. Sci.* **17**, 1431–1444.

Piao, S., Ciais, P., Huang, Y., Shen, Z., Peng, S., Li, J., Zhou, L., Liu, H., Ma, Y. & Ding, Y. 2010 The impacts of climate variability on water resources and agriculture in China. *Nature* **467** (7311), 43–51.

Pirkner, M., Dicken, U. & Tanny, J. 2013 Penman-Monteith approaches for estimating crop evapotranspiration in screen houses – a case study with table-grape. *Int. J. Biometeorol.* **58**, 725–737.

Sen, P. K. 1968 Estimates of the regression coefficient based on Kendall's tau. *J. Am. Stat. Assoc.* **63**, 1379–1389.

Tabari, H. 2010 Evaluation of reference crop evapotranspiration equations in various climates. *Water Resour. Manage.* **24**, 2311–2337.

Tabari, H. & Marofi, S. 2010 Changes of pan evaporation in the west of Iran. *Water Resour. Manage.* **25**, 97–111.

Teuling, A. J., Hirschi, M., Ohmura, A., Wild, M., Reichstein, M., Ciais, P., Buchmann, N., Ammann, C., Montagnani, L., Richardson, A. D., Wohlfahrt, G. & Seneviratne, S. I. 2009 A regional perspective on trends in continental evaporation. *Geophys. Res. Lett.* **36**, L02404.

Wang, W., Xing, W., Shao, Q., Yu, Z., Peng, S., Yang, T., Yong, B., Taylor, J. & Singh, V. P. 2013 Changes in reference evapotranspiration across the Tibetan Plateau: observations and future projections based on statistical downscaling. *J. Geophys. Res.* **118** (10), 4049–4068.

Xu, C., Gong, L., Jiang, T., Chen, D. & Singh, V. P. 2006 Analysis of spatial distribution and temporal trend of reference evapotranspiration and pan evaporation in Changjiang (Yangtze River) catchment. *J. Hydrol.* **327**, 81–93.

Xu, X., Liu, W., Scanlon, B. R., Zhang, L. & Pan, M. 2013 Local and global factors controlling water-energy balances within the Budyko framework. *Geophys. Res. Lett.* **40**, 6123–6129.

Yang, Q. Y., Zhang, B. P. & Zheng, D. 1988 On the boundary of the Loess Plateau. *J. Nat. Resour.* **3**, 9–15 (in Chinese).

Yang, D., Sun, F., Liu, Z., Cong, Z., Ni, G. & Lei, Z. 2006 Interpreting the complementary relationship in non-humid environments based on the Budyko and Penman hypotheses. *Geophys. Res. Lett.* **33**, L18402.

Yang, D., Sun, F., Liu, Z., Cong, Z., Ni, G. & Lei, Z. 2007 Analyzing spatial and temporal variability of annual water energy balance in nonhumid regions of China using the Budyko hypothesis. *Water Resour. Res.* **43**, W04426.

Yang, X., Ren, L., Singh, V. P., Liu, X., Yuan, F., Jiang, S. & Yong, B. 2012 Impacts of land use and land cover changes on evapotranspiration and runoff at Shalamulun River watershed, China. *Hydrol. Res.* **43** (1–2), 23–37.

Yang, L., Li, C., Wang, S. & Yang, W. 2014 Sensitive analysis of potential evapotranspiration to key climatic factors in Taohe River Basin. *Trans. Chinese Soc. Agric. Eng.* **30** (11), 102–109 (in Chinese with English abstract).

Yin, Y. H., Wu, S. H. & Dai, E. F. 2010 Determining factors in potential evapotranspiration changes over China in the period 1971–2008. *Chinese Sci. Bull.* **55**, 3329–3337.

Zhang, Y. L., Li, B. Y. & Zheng, D. 2002 A discussion on the boundary and area of the Tibetan Plateau in China. *Geogr. Res.* **21**, 1–8 (in Chinese).

Zhang, Y., Leuning, R., Chiew, F. H. S., Wang, E., Zhang, L., Liu, C., Sun, F., Peel, M. C., Shen, Y. & Jung, M. 2012 Decadal trends in evaporation from global energy and water balances. *J. Hydrometeor.* **13**, 379–391.

Zuo, D., Xu, Z., Yang, H. & Liu, X. 2012 Spatiotemporal variations and abrupt changes of potential evapotranspiration and its sensitivity to key meteorological variables in the Wei River basin, China. *Hydrol. Process.* **26** (8), 1149–1160.

First received 8 December 2015; accepted in revised form 4 May 2016. Available online 4 June 2016